Arch. Metall. Mater. **63** (2018), 4, 2061-2066

DOI: 10.24425/amm.2018.125143

A. URBAŃCZYK-GUCWA*#, A. BRZEZIŃSKA*, K. RODAK*

INFLUENCE OF SOLID SOLUTION AND AGING TREATMENT CONDITIONS ON THE FORMATION OF ULTRAFINE-GRAINED STRUCTURE OF CuCr0.6 ALLOY PROCESSED BY COMPRESSION WITH OSCILLATORY TORSION

The samples of the CuCr0.6 alloy in the solution treated and additionally in aging states were severely plastically deformed by compression with oscillatory torsion (COT) method to produce ultrafine – grained structure. The samples were processed by using process parameters as: frequency of torsion (f = 1.6 Hz), compression speed (v = 0.04 mm/s), angle torsion ($\alpha = \pm 6°$), height reduction (Δh = 7 mm). The total effective strain was ε_{ft} = 40. The microstructure has been analyzed by scanning transmission electron microscope (STEM) Hitachi HD-2300A equipped with a cold field emission gun at an accelerating voltage of 200 kV. The quantitative microstructure investigations as disorientation angles were performed using a FEI INSPECT F scanning electron microscope (SEM) equipped with a cold field emission gun and a electron backscattering diffraction (EBSD) detector. The mechanical properties were determined using MST QTest/10 machine equipped with digital image correlation (DIC). The COT processed alloy previously aged at 500°C per 2h shows high mechanical strength, ultimate tensile strength UTS: 521 MPa and yield tensile strength YS: 488 MP attributed to the high density of coherent precipitates and ultrafine grained structure.

Keywords: CuCr0.6 alloy, severe plastic deformation, ultrafine-grains, STEM

1. Introduction

Copper is a material generally used in electrical and electronic industry, but low strength properties limit the use of this material. Alloying of pure Cu increases tensile strength but decreases electrical conductivity [1]. The high mechanical properties of Cu alloys comparing to pure copper is achieved thanks to precipitation strengthening and strain hardening [2-7]. High mechanical properties and good electrical conductivity of CuCr alloys have been presented in [8-11].

Mentioned above properties can be improved by grain refinement via several plastic deformation (SPD) [12,13]. Most of the SPD processes are characterized by a cyclic deformation, which involves sudden change of strain path [14-16]. These methods are: accumulative roll banding (ARB), cyclic extrusion compression (CEC), multiple forged (MF) and equal channel angular pressing (ECAP) with sample rotation [17] and another presented in [18-20]. On the other hand, SPD processes offer deformation with a unchanged scheme of deformation. These methods include: equal channel angular pressing (ECAP) without sample rotation, high pressure torsion (HPT) and hydrostatic extrusion (HE).

One of the cyclic methods is compression with oscillatory torsion (COT). This method allows obtaing large deformation, and therefore grain refinement is possible [1]. This original method of deformation has been patented in Silesian University of Technology, Faculty of Materials Engineering and Metallurgy in Poland [21]. The basis of this method is the deformation of a massive sample by simultaneously applying compression and oscillatory torsion. Torsion straining is achieved by rotating the lower anvil, and compression is simultaneously achieved by a linear strain from the upper anvil (Fig. 1). The deformation path could be controlled by changing the proportions of the following parameters: torsion frequency f (0-1.8 Hz), torsion angle, α (0°-±8°), compression rate v (maximal –0.66 mm/s), and height reduction, Δh [mm].

The effect of heat treatment and second phase particles influence on the evolution of deformation structures [13] have been systematically studied in [10,22]. The authors of these works focused on small deformations or deformations carried out using conventional methods. Meanwhile, a new aspect in the approach to these issues may be grain refinement to the nano- and ultra-fine scale using SPD deformation processes in synergy with their heat treatment processes [4,12,23]. It is assumed that the secondary phases in the CuCr0.6 alloy deformed by compression with oscillatory torsion will favor obtaining nano- and ultra-fine grain structure [12].

In literature the effect of influence of fine particles on grain refinement in CuCr0.6 alloy is not well documented. In this study mechanical, electrical conductivity and microstructure of CuCr0.6 (C18200) alloys after applying different heat treatments and next COT deformation were investigated.

* SILESIAN UNIVERSITY OF TECHNOLOGY, FACULTY OF MATERIALS ENGINEERING AND METALLURGY, 8 KRASIŃSKIEGO STR., 40-019 KATOWICE, POLAND

Corresponding author: anna.urbanczyk-gucwa @polsl.pl

2. Research methodology

In this study, investigation were performed on copper alloys with addition of wt. % 0.6 Cr (C18200). The material was prepared by melting and alloying in open-air induction furnace. The ingots with the diameter of 50 mm were hot rolled into rods with the diameter of 10 mm. The following heat treatment processes were applied to the sample in order to vary the initial structure prior to the COT deformation:

1. Solution treatment at 1000°C for 3 h followed by quenching into iced water. In this article referred to as: S,
2. Solution and aging treatment at 500°C for 2h. Referred to as: S1,
3. Solution and aging treatment at 700°C for 24h. Referred to as: S2.

Specimens with three distinctly different initial conditions were deformed by using COT method. In our experiments, the compression with oscillatory torsion was carried out at values: torsion angle $\alpha = 6°$, true reduction $\Delta h = 7$ mm, compression rate $v = 0.04$ mm/s, torsion frequency $f = 1.6$ Hz and the total effective strain was $\varepsilon_{fi} = 40$.

All tests by using the COT method were conducted at room temperature. The samples in heat treated conditions and next deformed by COT are referred to as: S+COT; S1+COT and S2+COT.

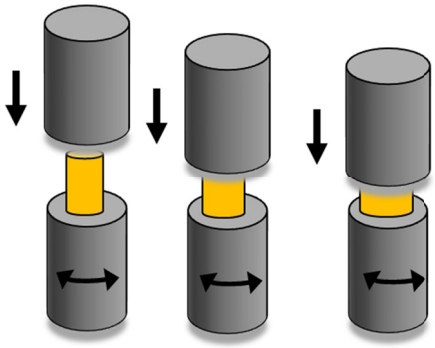

Fig. 1. Scheme of COT method

The microstructure has been analyzed by scanning transmission electron microscope (STEM) Hitachi HD-2300A equipped with a cold field emission gun at an accelerating voltage of 200 kV. The quantitative investigation of the ultrafine-grained structure (character of grain boundaries) was performed using a FEI INSPECT F scanning electron microscope (SEM) equipped with a cold field emission gun and a electron backscattering diffraction (EBSD) detector. SEM specimens were polished by using an ion thinning device (PECS) manufactured by Gatan, Inc. Quantitative studies of the grain/subgrain size based on the STEM images were performed using the "MET-ILO" software package [24]. The mechanical properties of the alloys were characterized by microhardness measurements. The Vickers hardness was measured on an electrolytically polished surface of the samples by means of Future-Tech. Corp. Fm-800 load applied for 15 s was ensured for these measurements.

The hardness values were taken as the average of a minimum of 10 measurements. The International Annealed Copper Standard (IACS) establishes a standard for the conductivity of commercially pure annealed copper. According with establishment at 20°C, commercially pure, annealed copper has a resistivity of 5.8001×10^7 S/m. A conductivity of 5.8001×10^7 S/m may be expressed as 100% IACS at 20°C. All other conductivity values are related back to this standard value of conductivity for annealed copper.

The mechanical properties were determined on an MST QTest/10 machine equipped with digital image correlation (DIC). The tensile tests were performed at room temperature at an initial strain rate 1×10^{-3} s^{-1}. Mini tensile specimens with a total length and thickness of 8.6 mm and 0.3 mm, respectively, were used to measure the mechanical properties. The tensile specimens were cut in the planes parallel to the sample axis. The micro specimens were produced by an electrical-sparking machine to eliminate the heat – affected zone. Four tensile tests were performed on each sample and the average values and standard deviations were calculated. All the tests were performed at room temperature.

3. Results

Figure 2 show the microstructure of CuCr0.6 alloy after solution treatment. Microstructure is characterized by the presence of undissolved equiaxial Cr precipitates in Cu matrix. The average diameter between precipitates is about 0.7 µm and average distance of particles is about 2.5 µm (Fig. 2a). Based on STEM/EDS investigations it has been shown, that the precipitates are rich in P (Fig. 2b). Phosphorus was added as an antioxidant during casting. The initial grain size of the specimen in the solution treatment conditions was determined as 72 µm.

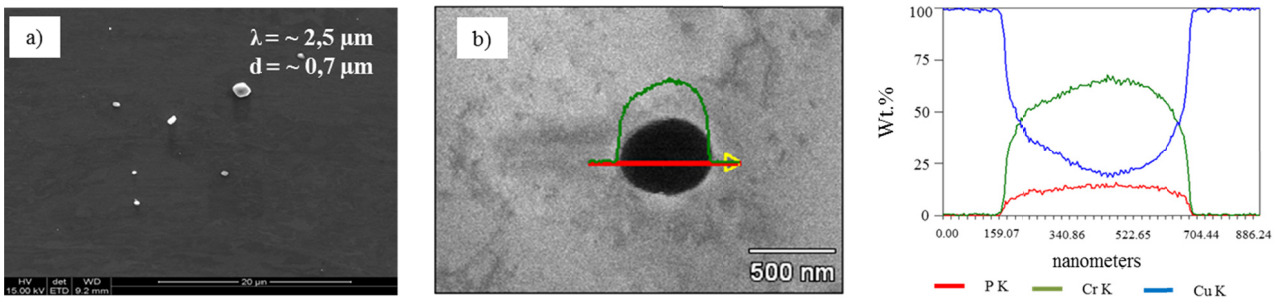

Fig. 2. Microstructure of CuCr0.6 alloy after solution treatment a), EDS investigation of particles b)

Fig. 3a,b shows the microstructure of CuCr0.6 alloy after solution and aging treatment followed at 500°C for 2 h (S1) and at 700°C for 24 h (S2) respectively. Aging treatment at 500°C for 2 h results in the formation of coherent Cr precipitates within the matrix (Fig. 3a). The average diameter of these particles is about 20 nm. With prolonged aging temperature and time, the precipitates lose coherence with matrix (Fig. 3b) and amount of the particles within the matrix decreases (spacing between particles increase). The size of these particles varies between 100 to 500 nm (Fig. 3b).

Figures 4-6 show microstructure CuCr0.6 alloy after heat treatment and deformation with distribution of average grain/subgrain size and shape index. Additionally, quantitative results of disorientation measurements by using SEM/EBSD are presented in Fig. 7. Most of the grains/subgrains in S+COT state contain low density of dislocations. Although there are observed grains/subgrains with high density of dislocations (Fig. 4a). In S1+COT state there are visible grains/subgrains with high density of dislocations inside grains and with grain boundaries in non-equilibrium state (Fig. 5a). Grains/subgrains in S2+COT state are near free from dislocations (Fig. 6a). The refined microstructure of deformed samples is characterized by a mixture of equiaxed and eloganted subgrains/grains with the shape index in the range from 0.3 to 0.4. Dimension of grains and subgrains in S+COT and S2+COT states are nearly the same (about ~0.4 μm). The average diameter of grain/subgrain for S1+COT state is about 0.3 μm.

The fraction of HABs in COT processed samples in states S1+COT and S2+COT is higher than in S+COT state (Fig. 7). The maximal fraction of HABs about 30% were obtained for S1+COT state. This means that higher number of LABs are still observed in samples after deformation. It should be noted that fractions of HABs, MABs and LABs for S+COT and S2+COT are similar although in S2+COT state fraction frequency of HABs and MABs is slightly higher.

Results of hardness and electrical conductivity measurements for CuCr0.6 alloy after heat treatment and heat treatment with COT deformation are presented in Fig. 8 a and b respectively.

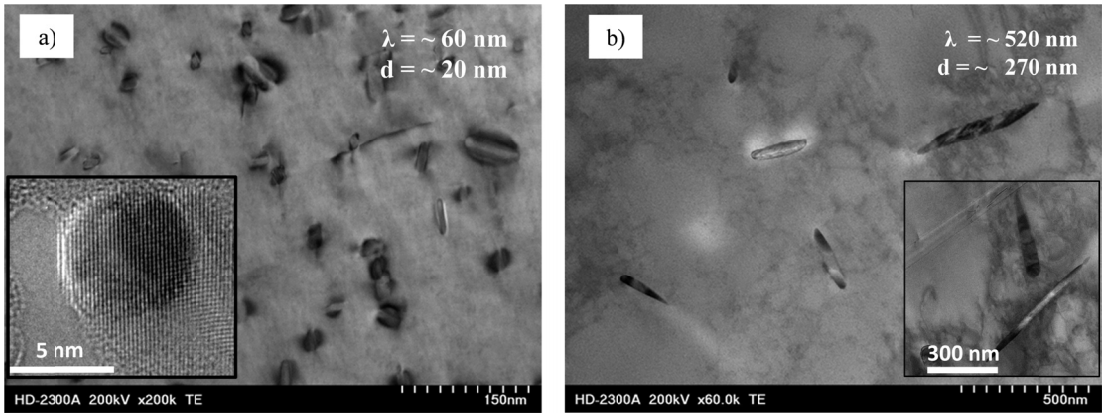

Fig. 3. Microstructure of CuCr0.6 alloy after S1 a), and microstructure of CuCr0.6 alloy after S2 b)

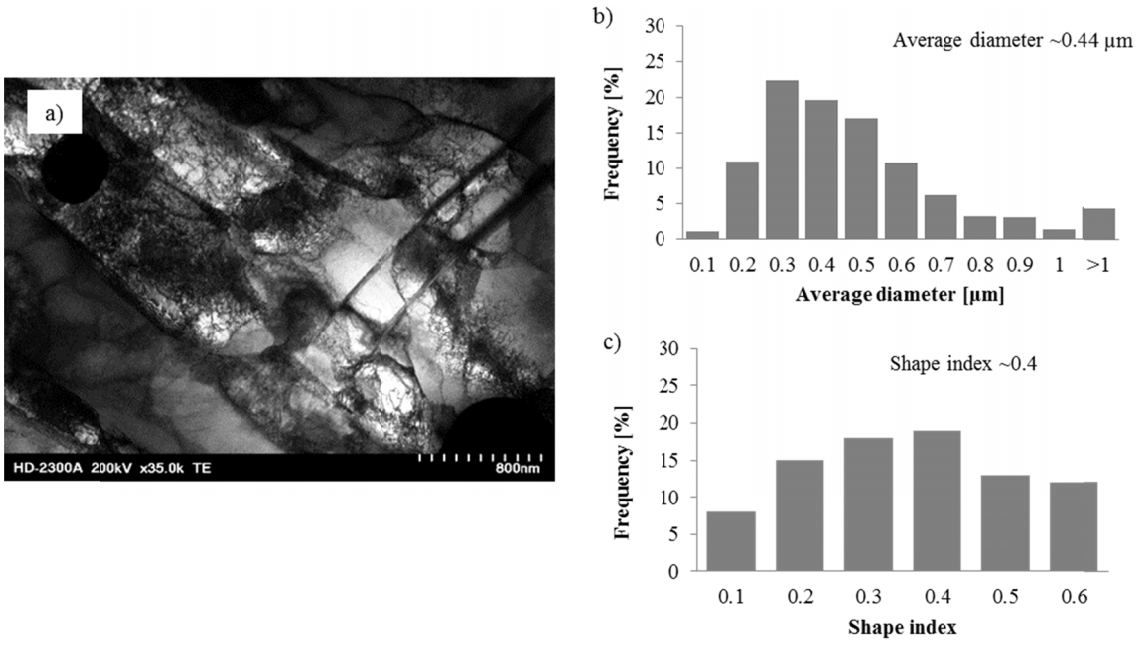

Fig. 4. Microstructure of CuCr0.6 alloy for S1+COT a), distribution of average grain/subgrain size b) distribution of shape index

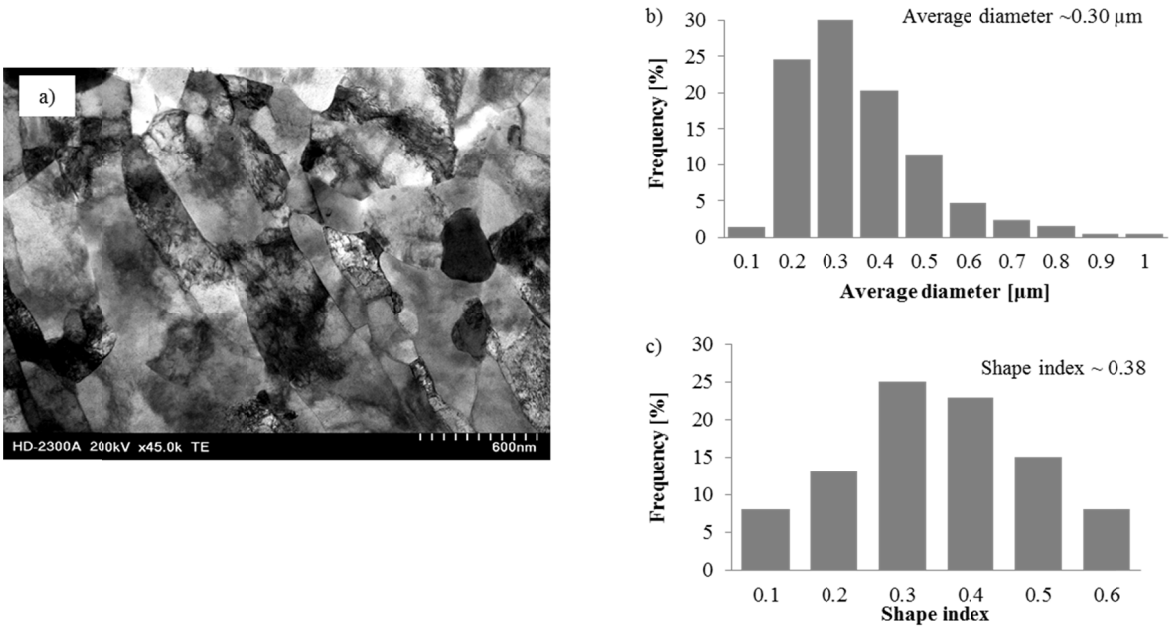

Fig. 5. Microstructure of CuCr0.6 alloy for S1+COT a), distribution of average grain/subgrain size b) distribution of shape index

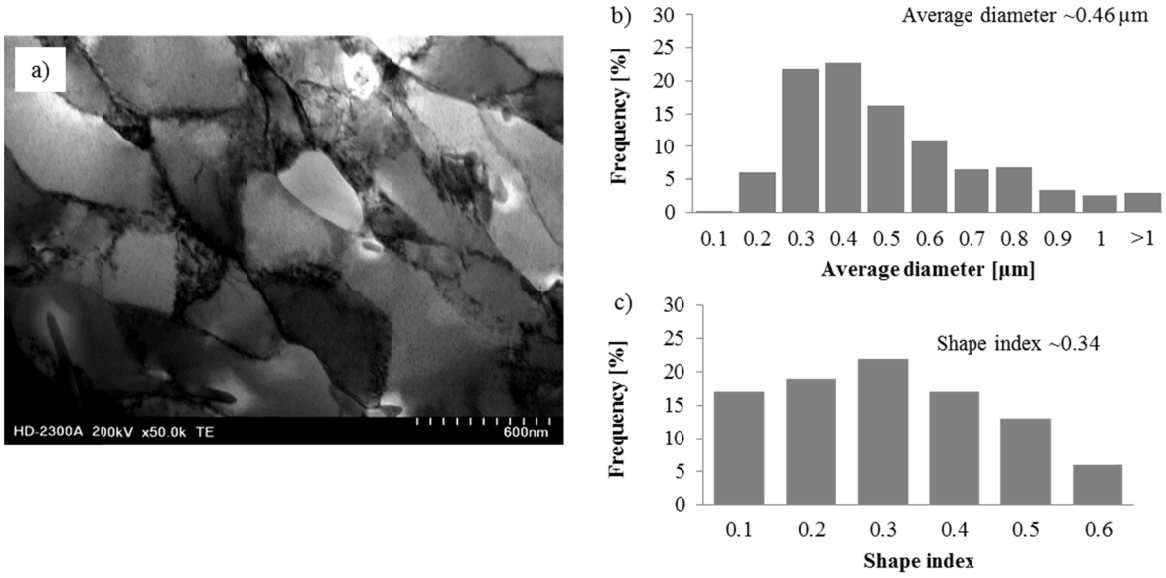

Fig. 6. Microstructure of CuCr0.6 alloy for S2+COT a), distribution of average grain/subgrain size b) distribution of shape index

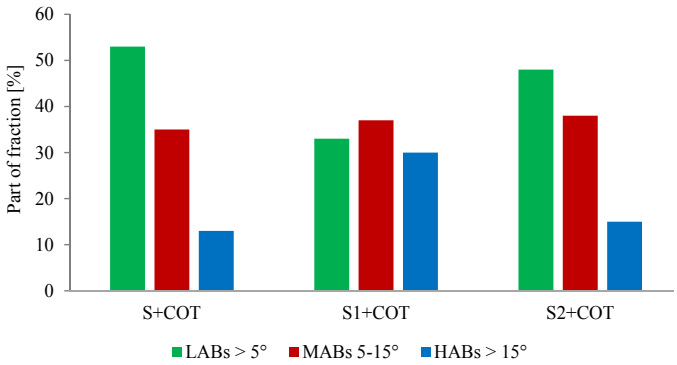

Fig. 7. Fraction of high angle boundaries (HABs), medium angle boundaries (MABs) and low angle boundaries (LABs)

After heat treatment maximal hardness of about 134 HV0.2 have been obtained for S1 state. For S and S2 state hardness was 42 HV0.2 and 55 HV0.2 respectively. Heat treatment and deformation results in a significant increase in hardness compared with samples after applying only heat treatment. In S1+COT state the hardness was 164 HV0.2. For S+COT and S2+COT states the hardness were 123 HV0.2 and 120 HV0.2 respectively. The significant difference in the electrical conductivity due to COT processing between the samples with and without the coherent precipitations (Table 1) is another interesting feature of our results. As shown in Table 1, the electric conductivity of the samples processed by quenching and COT treatment reached about 40% IACS. This value is quite poor and is not acceptable for electrome-

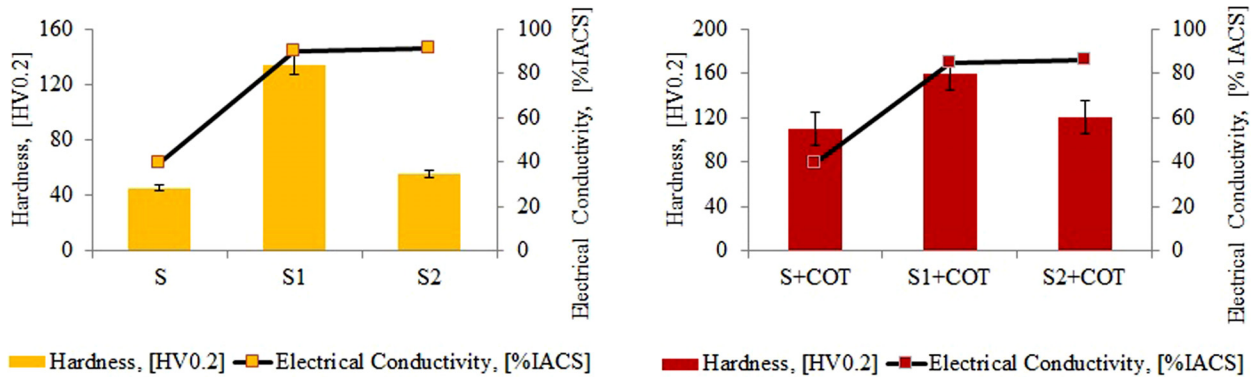

Fig. 8. Hardness of CuCr0.6 alloy for heat treatment a) after deformation b)

chanical applications. The electrical conductivity of the samples processed by aging and COT treatment is satisfactory and is in 85-86% range. The highest electrical conductivity was observed in the COT-processed samples with aging structure where the atoms of the alloying elements were found in the form of precipitates. This was facilitated by a decrease in the content of the chromium alloying element in the crystal lattice. It should be noted that electrical conductivity is more sensitive to alloying element in the crystal lattice than to defects observed after deformation. In our experiments while the recovery of the defect structure accompanied by a decrease of the dislocation density certainly contributes to the electrical conductivity increase, this effect appears to be minimal compared to influence of the alloying elements.

Mechanical properties of CuCr0.6 alloys were measured by uniaxial tensile tests as shown in Table 1 and Fig. 9. In CuCr0.6 alloy after solution treatment and deformation (S+COT) the YS and UTS were (347 MPa) and (353 MPa) respectively. The best results in strength properties (UTS: 521 MPa, YS: 488 MPa,) in CuCr0.6 alloy were obtained for S1+COT state. In S2+COT state is an increase of the UTS (~20 MPa) compared with S+COT state. Values of YS are quite comparable for S+COT and S2+COT state. The maximum in ductility is observed for samples in the initial state. Elongation to fracture (A_c) and uniform elongation (A_{gt}) (elongation before necking) is about 26% and 22% respectively. The alloys after COT deformation shows elongation to fracture (A_c) in the range (7%-10%). These

TABLE 1

Measured mechanical parameters: yield strength (YS), ultimate tensile strength (UTS), uniform elongation (A_{gt}), and elongation to fracture (A_c) of deformed CuCr0.6 alloy

Material state	YS (MPa)	UTS (MPa)	A_{gt} (%)	A_c (%)	HV0.2	IACS (%)
Quenching	97 ± 4	214 ± 5	22.5 ± 1	26.0 ± 1	43 ± 6	40 ± 1
Quenching + COT	347 ± 8	353 ± 7	1.0 ± 0.2	7.2 ± 1.5	123 ± 7	40 ± 1
Aging at 500°C + COT	488 ± 14	521 ± 12	1.6 ± 0.3	7.8 ± 1.4	164 ± 12	85 ± 1
Aging at 700°C + COT	343 ± 7	372 ± 6	2.86 ± 0.4	9.9 ± 1.5	120 ± 4	86 ± 1

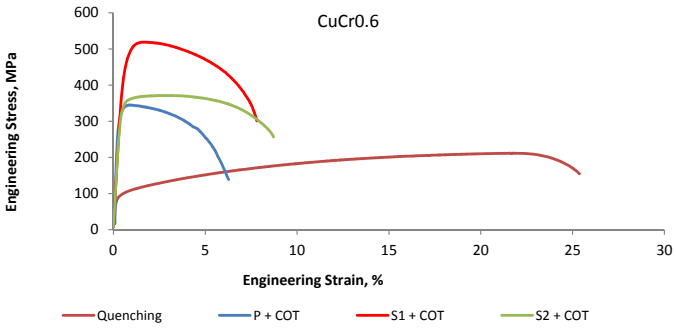

Fig. 9. Effect of COT deformation on the tensile properties of the CuCr0.6

results indicate that the processed sample may show an enhanced elongation to fracture. Uniform elongation (A_{gt}) obtained for the deformed alloy was considerable smaller, the values were in the range (1%-3%). In the samples after compression with oscillatory torsion there are observed a strong increase in YS and UTS with significant decrease in A_{gt} and A_c compared to the material in initial state (Table 1).

4. Discussion

Basing on the performed investigations it is evident that only the combination of grain size strengthening with precipitation hardening (aging at 500°C/2 h) significantly affect the strength of CuCr0.6 alloy (Fig. 9). The formation of a UFG microstructure significantly depends on the size of second-phase precipitates, precipitate morphology and their distribution within the Cu matrix. The enhanced strength of CuCr0.6 alloy in S1+COT state is attributed to structural strengthening due to the formation of a reasonably equiaxed UFG microstructure with average grain sizes of 0.3 μm (Fig. 5) and with the fraction of high angle boundaries (HABs) which reaches about 30% (Fig. 7). Obtained UFG structures effectively accumulate a high density of dislocations during deformation thanks to coherent precipitates, which explains high mechanical properties (Fig. 9).

Structures evolved under COT in S+COT state are delimited especially by low-angle boundaries (LABs) (Fig.7). The lattice dislocations arrange into cells and form the dislocation network

within initial grains. Very often grains/subgrains look like recovered with low dislocation density in grain boundaries. Increase in YS is attributed to a combination of dislocation strengthening with solid solution strengthening (Fig. 9). However, a remarkable reduction in ductility Fig. 9 and Table 1 is the main disadvantage.

Uniform elongation for S+COT state does not exceed 1% (Table 1). It seems that low value of uniform elongation is the main disadvantage of alloy in S+COT state. Obtained microstructures are not homogeneous and contain recovery areas and subgrains with high dislocation density (Fig. 4a).

Increase in ductility and uniform elongation takes place due to the formation of UFG structure and elimination of precipitation-free zones [10]. Additionally according to the literature, the improvement in the ductility can be achieved due to an increasing number of HABs and the presence of fine dislocation-free grains with different orientations [25]. These conditions are typically observed for S2+COT state, where stable precipitations of Cr obtained during over-aging process effectively suppress the migration of MABs and HABs (Fig. 6a). Increasing the number of medium and high-angle boundaries (Fig. 7) leads to significant increase in ductility (Fig. 9). In S2+COT state the microstructure consists of well- defined grains/subgrains with the low dislocation density inside the grains/subgrains (Fig. 6a). For these types of microstructures the tendency to strain localization is weakened. The formation of coarse particles of the stable Cr precipitates on boundaries of micron scale grains and even within interiors of these grains (Fig. 6a) leads to decrease in strength of the alloy.

5. Conclusions

1. COT deformation causes formation of ultrafine-grained structure of CuCr0.6 alloy.
2. The obtained results demonstrate the capability of COT processing of CuCr0.6 alloy in aging state for reaching high mechanical properties and high electrical conductivity.
3. The best result in strength properties (UTS: 521 MPa, YS: 488 MPa) were obtained for sample S1+COT. This effect can be explained by the high dislocation density and decrease in grain/subgrain size due to pinning effect of coherent precipitates.
4. The COT process for the S1+COT state can promote increase in the fraction of HABs.

Acknowledgements

The work was supported by the National Science Centre of Poland (project No. UMO-2013/09/B/ST8/01695).

REFERENCES

[1] L. Kommel, A. Pokatilov, IOP Conf. Ser. Mater. Sci. Eng. **63**, (2014). DOI: 10.1088/1757-899X/63/1/012169

[2] M. Kawasaki, H.J. Lee, J. Il Jang, T.G. Langdon, Rev. Adv. Mater. Sci. **48**, 13-24 (2017).

[3] I. Sabirov, M.Y. Murashkin, R.Z. Valiev, Mater. Sci. Eng. A **560**, 1-24 (2013). DOI: 10.1016/j.msea.2012.09.020

[4] D.V. Shangina, N.R. Bochvar, M.V. Gorshenkov, H. Yanar, G. Purcek, S.V. Dobatkin, Mater. Sci. Eng. A **650**, 63-66 (2016). DOI: 10.1016/J.MSEA.2015.10.008

[5] A. Vinogradov, Y. Suzuki, T. Ishida, K. Kitagawa, V.I. Kopylov, Mater. Trans. **45**, 2187-2191 (2004). DOI: 10.2320/matertrans.45.2187

[6] R.Z.V. R.K. Islamgaliev, K.M. Nesterov, J. Bourgon, Y. Champion, J. Appl. Physic **115**, 194301-194304 (2014).

[7] P. Bazarnik, M. Lewandowska, M. Andrzejczuk, K.J. Kurzydlowski, Mater. Sci. Eng. A **556**, 134-139 (2012). DOI: 10.1016/J.MSEA.2012.06.068

[8] N. Liang, J. Liu, S. Lin, Y. Wang, J.T. Wang, Y. Zhao, Y. Zhu, J. Alloys Compd. **735**, 1389-1394 (2018). DOI: 10.1016/J.JALLCOM.2017.11.309

[9] Z. Rdzawski, J. Stobrawa, W. Głuchowski, J. Sobota, Arch. Metall. Mater. **59**, (2014). DOI: 10.2478/amm-2014-0106

[10] K.X. Wei, W. Wei, F. Wang, Q.B. Du, I. V. Alexandrov, J. Hu, Mater. Sci. Eng. A **528**, 1478–1484 (2011). DOI: 10.1016/j.msea.2010.10.059

[11] W. Głuchowski, J. Domagała-Dubiel, J. Sobota, J. Stobrawa, Z. Rdzawski, Arch. Mater. Sci. Eng. **60**, 53-63 (2013).

[12] K. Rodak, A. Brzezińska, R. Molak, Mater. Sci. Eng. A (2018). DOI: 10.1016/j.msea.2018.03.077

[13] K. Rodak, A. Urbańczyk-Gucwa, M.B. Jabłońska, Arch. Civ. Mech. Eng. **18**, (2018). DOI: 10.1016/j.acme.2017.07.001

[14] A. Vinogradov, T. Ishida, K. Kitagawa, V.I. Kopylov, Acta Mater. **53**, 2181-2192 (2005). DOI: 10.1016/J.ACTAMAT.2005.01.046

[15] P.L. Sun, C.Y. Yu, P.W. Kao, C.P. Chang, Scr. Mater. **47**, 377-381 (2002). DOI: 10.1016/S1359-6462(02)00117-3

[16] Bochniak W. Korbel A., Mater. Sci. Technol. **16**, 664-674 (2000).

[17] M. Lewandowska, Oficyna Wydawnictwa Politechniki Warszawskiej, (2006)

[18] K. Rodak, J. Pawlicki, J. Mater. Sci. Technol. **27**, 1083-1088 (2011). DOI: 10.1016/S1005-0302(11)60190-4

[19] P.Z. Rodak K., Molak R.M., Phys. Status Solidi C-Curent Top. Solid State Phys. **7**, 1351-1354 (2010).

[20] Z. Cyganek, K. Rodak, F. Grosman, Arch. Civ. Mech. Eng. **13**, 7-13 (2013). DOI: 10.1016/J.ACME.2012.10.008

[21] Patent no. PL 203220 B1, b.d.

[22] Z.M. Rdzawski, J. Stobrawa, W. Głuchowski, J. Achiev. Mater. Manuf. Eng. **33**, 7-18 (2009).

[23] H. Cao, J.Y. Min, S.D. Wu, A.P. Xian, J.K. Shang, Mater. Sci. Eng. A **431**, 86-91 (2006). DOI: 10.1016/J.MSEA.2006.05.081

[24] J. Szala, Computer Quantitative Metallography: MET-ILO V.3.0., Department, Silesian Univeristy of Technology, 1997.

[25] S.V. Dobatkin, J. Gubicza, D.V. Shangina, N.R. Bochvar, N.Y. Tabachkova, Matt. Lett. **153**, 5-9 (2015). DOI: 10.1016/j.matlet.2015.03.144